Supporting Information

Self-Supported Co-Mn Oxide Porous Nanosheets Electrode for Enhanced Oxygen Evolution and Seawater Zinc-Air Batteries

*Zheng Sun[‡a], Shi-Fang Yang[‡a], Xu Liu [b], Ying Wang[a, *], Wang-Dong Lu[c, *], Peng Yu[a, *]*

[a] Key Laboratory for Photonic and Electronic Bandgap Materials, Ministry of Education, School of Physics and Electronic Engineering, Harbin Normal University, Harbin, 150025, China.

[b] Department of Chemistry, College of Arts and Science, Northeast Agricultural University, Harbin 150030, China.

c Key Laboratory of Modern Measurement & Control Technology, Ministry of Education, Beijing Information Science & Technology University, Beijing 102206, China.

* Corresponding authors. E-mail addresses: wangying_10_16@126.com (Y. Wang); wdlu@bistu.edu.cn (W. Lu); yupeng@hrbnu.edu.cn (P. Yu).

‡ Equally contributed to this work..

EXPERIMENTAL SECTIONS

1 Synthesis of CoMnO/CC Catalysts

The CoMnO/CC catalyst was fabricated via cathodic electrodeposition followed by ligand modification and thermal treatment. Electrodeposition was performed using a standard three-electrode system on a CHI 660E electrochemical workstation. with carbon cloth (1 cm × 2 cm) served as the working electrode, a platinum sheet as the counter electrode, and a saturated calomel electrode (SCE) as the reference electrode. First, manganese-containing species were deposited onto the pretreated CC from a 0.1 M manganese acetate and sodium sulfate mixed solution at a constant potential of 1 V for 270 s. Subsequently, cobalt-containing species were deposited from a 0.1 M $Co(NO_3)_2$ solution at -1 V for 360 s. After electrodeposition, the CC was rinsed thoroughly with deionized water and ethanol each for three times, then dried at 50 ^oC to obtain the CoMn-Precursor. After electrodeposition, the mass ratio of manganese to cobalt is approximately 1:1.

The as-prepared CoMn-Precursor was immersed in a 1 M 2-methylimidazole methanol solution for 18 h at room temperature. After immersion, the sample was rinsed with deionized water and ethanol each for three times and dried at 50 ^oC to yield the CoMn-18-precursor. Finally, the CoMn-18-Precursor was annealed in a tube furnace under N_2 atmosphere with a heating rate of 5 ^oC /min and maintained at 500 ^oC at for 2 h, resulting in the CoMnO/CC catalyst.

For comparison, monometallic reference catalysts (CoO/CC and MnO/CC) were synthesized via the same procedure but with electrodeposition of only cobalt nitrate or manganese acetate, respectively, followed by ligand immersion and annealing. Additionally, a series of comparative samples with different ligand immersion times

were prepared, denoted as CoMnO/CC-X (where X represents the immersion time).

2 Electrochemical Measurements

Electrochemical measurements were performed on a CHI 660E electrochemical workstation using a standard three-electrode system in 1 M KOH solution at room temperature. The CoMnO/CC catalyst served as the working electrode, while an Ag/AgCl electrode (saturated KCl) and a platinum sheet were used as the reference and counter electrodes, respectively. Linear sweep voltammetry (LSV) was employed to record the OER polarization curves at a scan rate of 5 $mV \cdot s^{-1}$ with IR compensation. All potentials were calibrated to the reversible hydrogen electrode (RHE) using the equation: $E(RHE) = E_{(Ag/AgCl)} + 0.059 \times pH + 0.197$ V, unless otherwise stated. The electrochemical active surface area (ECSA) was estimated from the electrochemical double-layer capacitance. Electrochemical impedance spectroscopy (EIS) measurements were conducted at 1.55 V vs. RHE over the frequency range of 5 mHz to 100 kHz. The cycle performance of the catalytic electrode was evaluated by chronopotentiometry at 10 $mA \cdot cm^{-2}$ for OER.

3 Assembly and Testing of Zinc-Air Batteries

Rechargeable ZABs were assembled at room temperature with the as-prepared catalysts as bifunctional air cathodes, zinc foil as the anode, and a mixed solution of 6.0 M KOH and 0.2 M $Zn(Ac)_2$ as the electrolyte. For comparison, commercial Pt/C-RuO_2 composite (mass ratio 1:1) was used as the reference cathode catalyst. The Pt/C-RuO_2 ink was prepared by ultrasonically dispersing 5 mg Pt/C and 5 mg RuO_2 in 300 μL ethanol for 30 min, followed by adding 100 μL of 5% Nafion solution and further ultrasonic treatment for 30 min. The resulting ink was uniformly drop-cast onto a carbon cloth and dried at 60 °C for 1 h. The active material (Co-Mn oxide) loading on the carbon cloth substrate is strictly controlled at 2 mg cm^{-2} throughout all

experiments.

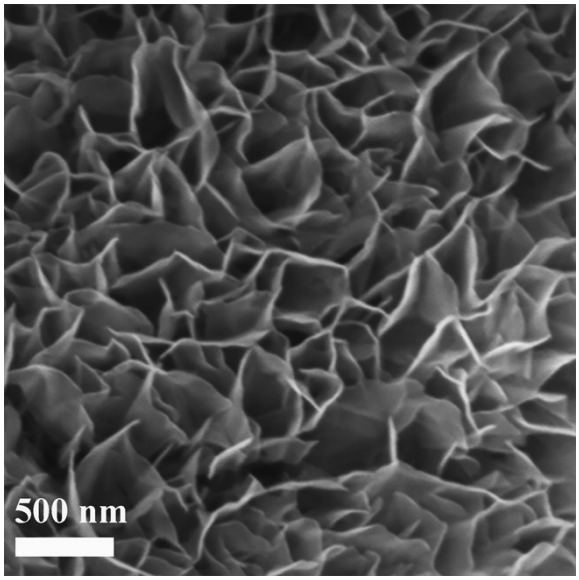

Fig. S1 SEM image of CoMn-precursor.

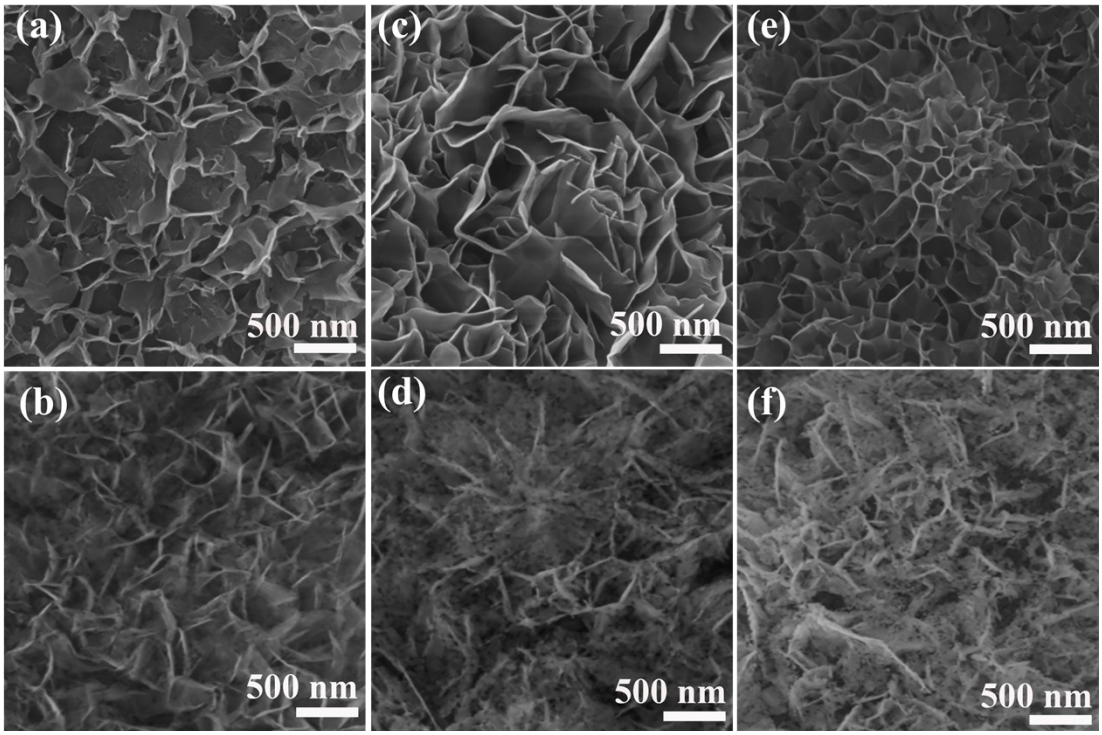

Fig. S2 SEM images of (a) CoMn/CC-3-Precursor, (b) CoMn/CC-3-Precursor, (c) CoMn/CC-6-Precursor, (d) CoMn/CC-6, (e) CoMn/CC-12-Precursor, (a) CoMn/CC-12.

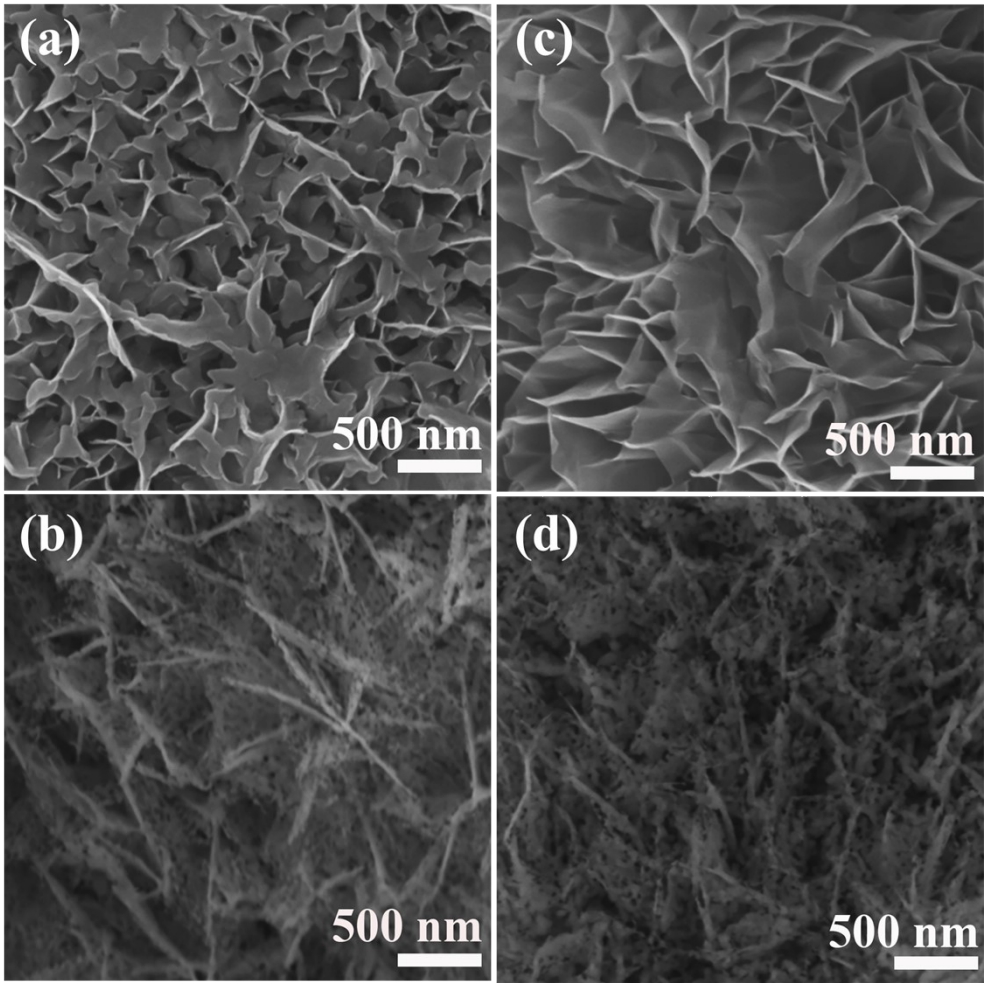

Fig. S3 SEM images of (a) CoMn/CC-24-precursor, (b) CoMn/CC-24, (c) CoMn/CC-30-precursor, (d) CoMn/CC-30.

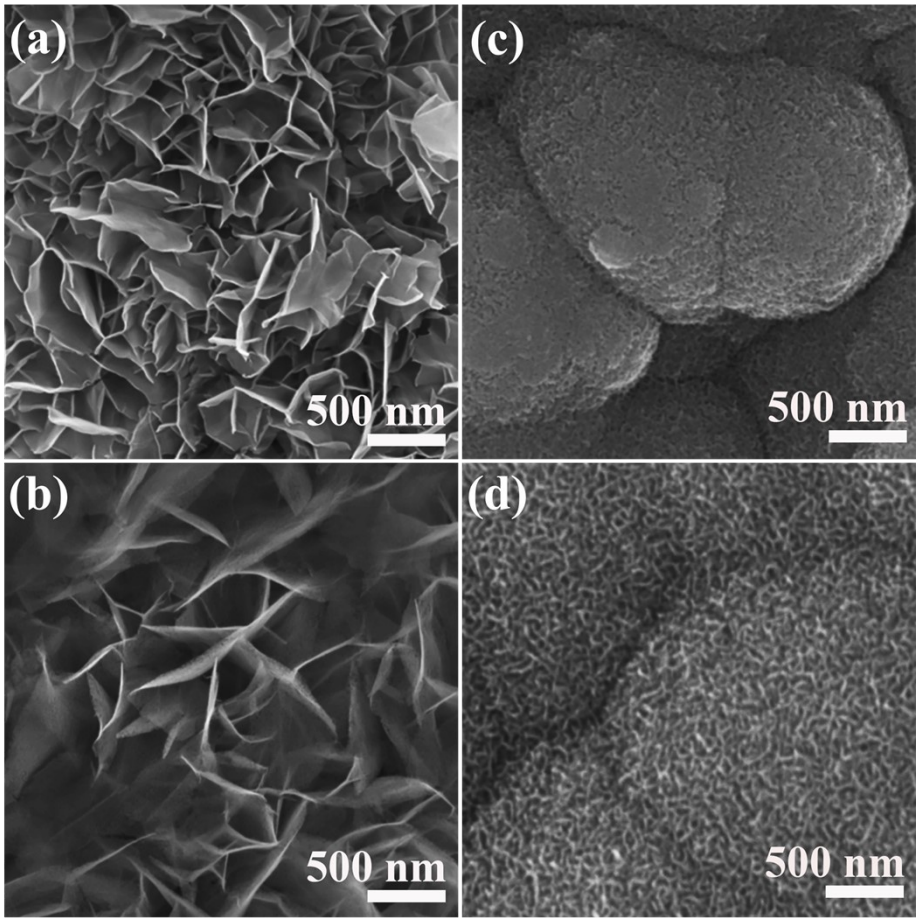

Fig. S4 SEM images of (a) CoO/CC-18-Precursor; (b) CoO/CC; (c) Mn/CC-18-Precursor; (d) MnO/CC.

Catalyst	Mn	Co	C	O
CoMnO/CC	38.64	36.87	19.82	4.58

Table S1. Atomic content percentage determined by SEM-EDS

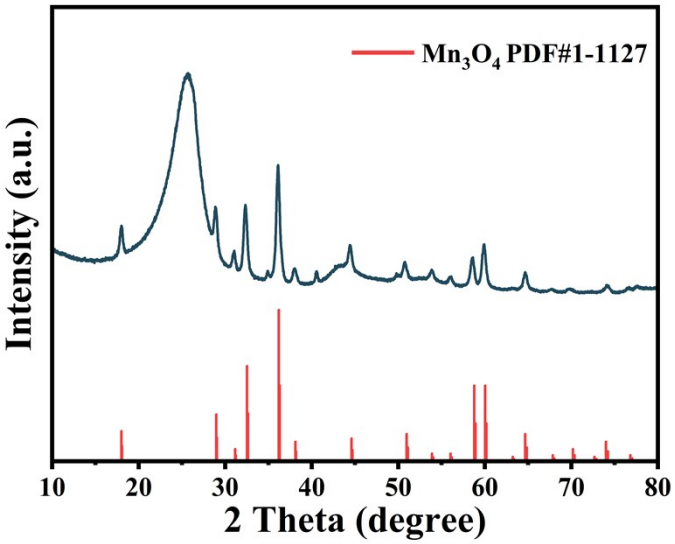

Fig. S5 XRD patterns of MnO/CC.

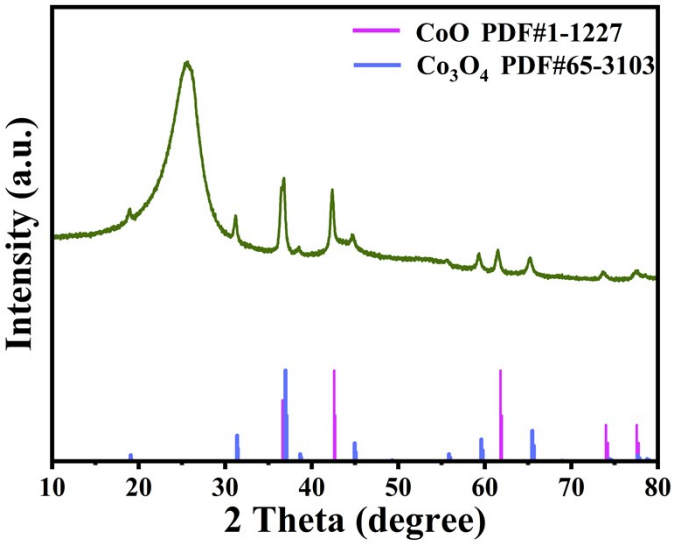

Fig.S6 XRD patterns of CoO/CC.

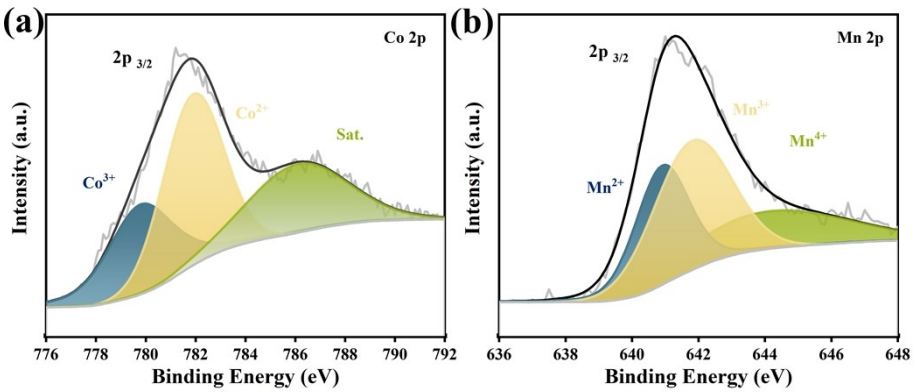

Fig.S7 XPS spectroscopy of CoO/CC and MnO/CC.

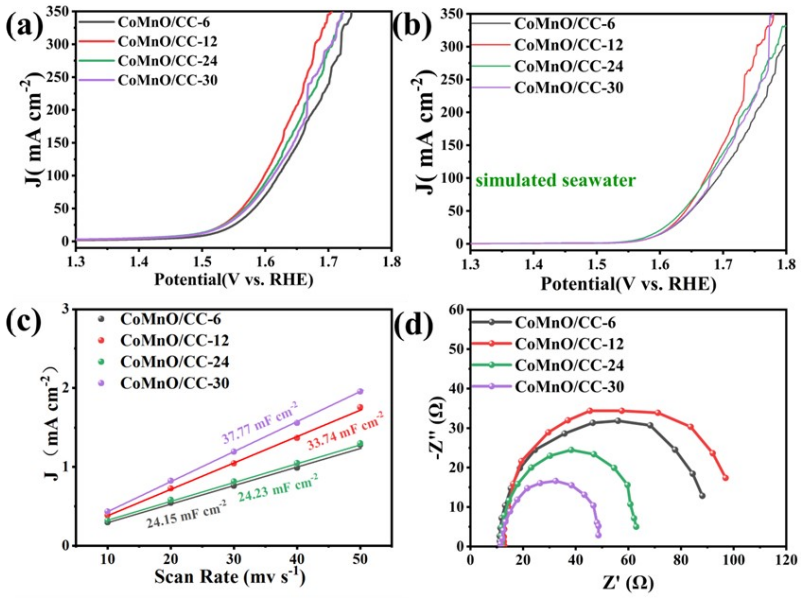

Fig. S8. OER LSV curves of samples with different deposition times. (a) 1 M KOH; (b) 1 M KOH simulated seawater; (c) Double-layer capacitance (C_{dl}) values of corresponding samples; (d) Electrochemical impedance spectroscopy (EIS) spectra of corresponding samples.

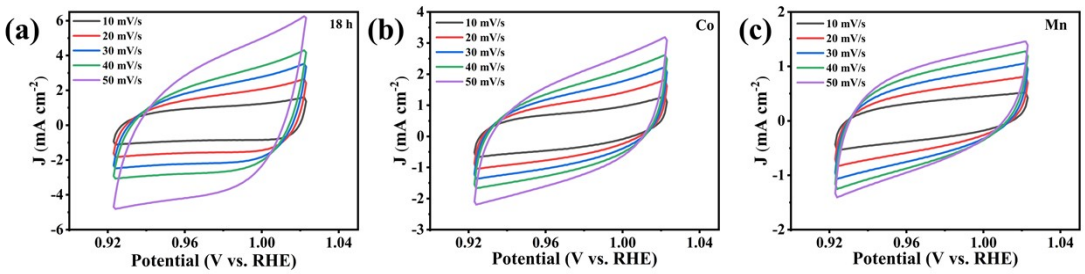

Fig. S9 CV curves of (a) CoMnO/CC; (b) CoO/CC; and (c) MnO/CC at different scanning rates.

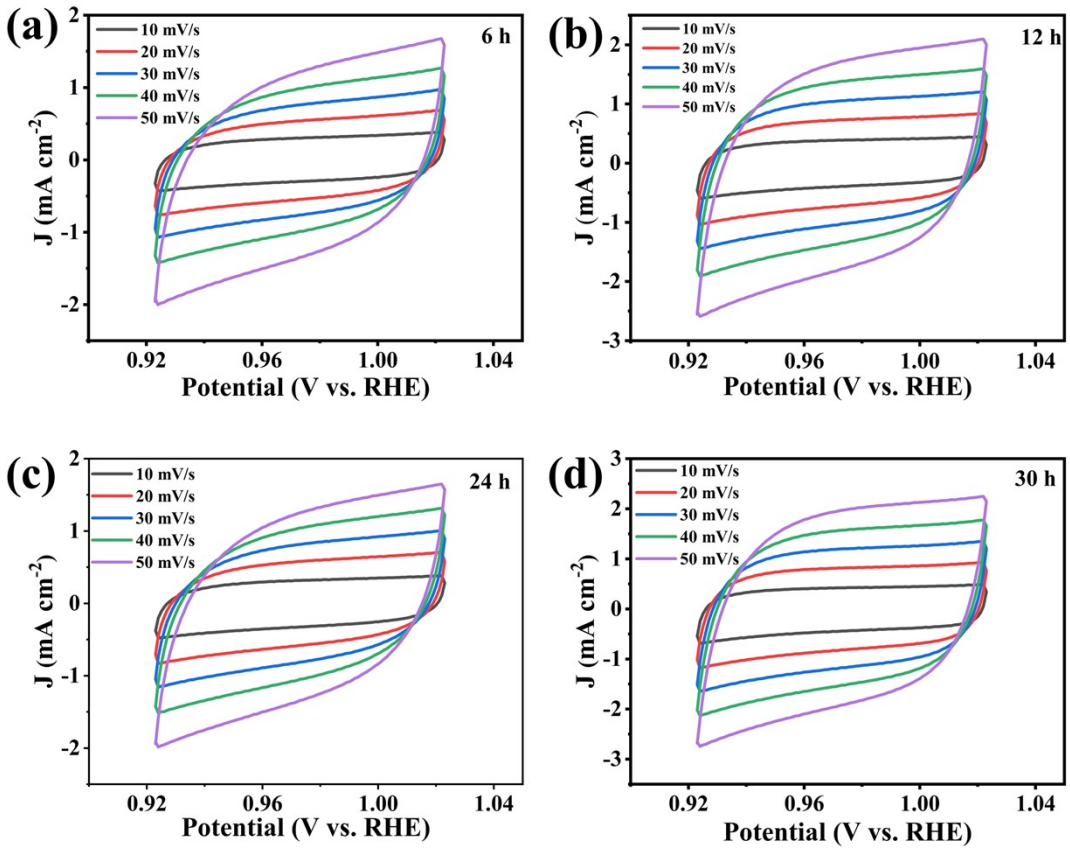

Fig. S10 CV curves of (a) CoMnO/CC-6; (b) CoMnO/CC-12; (c) CoMnO/CC-24; and (c) CoMnO/CC-30 at different scanning rates.

Table S2. Performance comparison of self-supporting electrocatalysts for zinc–air batteries.

Material	Overpotential ($10\ mA \cdot cm^{-2}$)	Tafel slope ($mV \cdot dec^{-1}$)	References
CoP@CC	300	124	[S1]
NC-Co_3O_4/CC	210	79.6	[S2]
Co/CeO_2-NCNA@CC	350	98	[S3]
CoO@PCNAs@CC	470	171	[S4]
FeNi@NBCNTs/CC	290	85.7	[S5]
W, Cr-Co_3O_4/NF	347	136.66	[S6]
CoP/Co_3O_4/N-CNFs-370-1:40	287	88.3	[S7]
np-CoCrFeNiNb	251	42.7	[S8]
NCA/FeRu	263	83.3	[S9]
Co1Cu1@NCNT/CC	263	53.1	[S10]
CoMnO/CC	243	66.45	This work

The OER overpotential of CoMnO/CC is lower than that of most catalysts such as CoP@CC (300 mV), Co/CeO_2 (350 mV), and CoO@PCNAs@CC (470 mV), and only slightly higher than that of NC-Co_3O_4/CC (210 mV). Meanwhile, the Tafel slope of this catalyst is 66.45 $mV \cdot dec^{-1}$, ranking among the leading levels among all comparative catalysts, which reflects faster OER reaction kinetics. This Tafel slope is only higher than that of np-CoCrFeNiNb (42.7 $mV \cdot dec^{-1}$), but significantly lower than that of similar materials like CoP@CC (124 $mV \cdot dec^{-1}$) and CoO@PCNAs@CC (171 $mV \cdot dec^{-1}$).

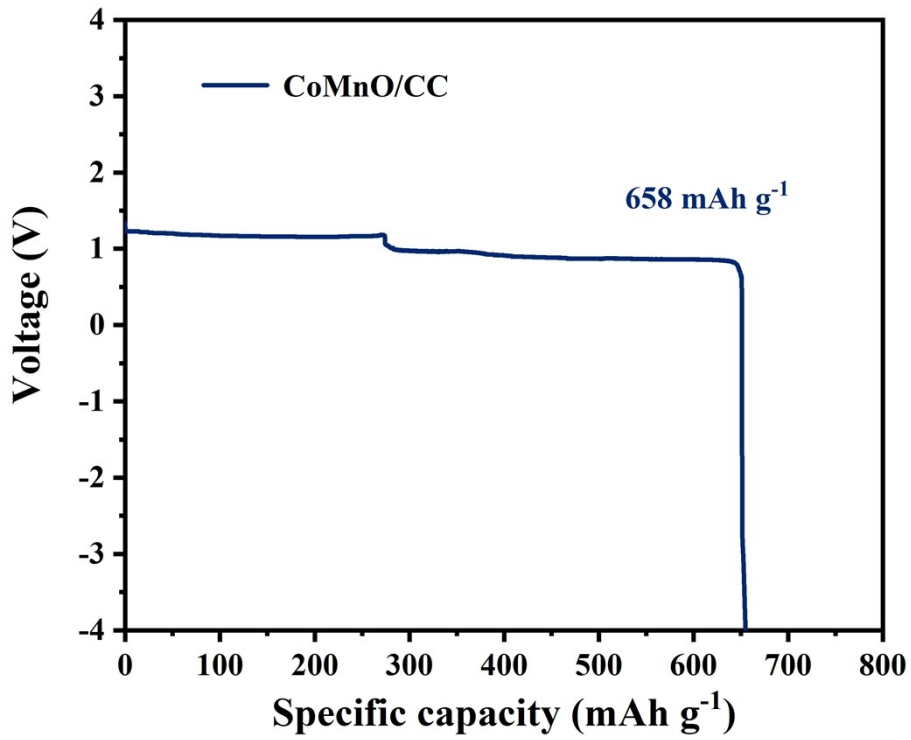

Fig. S11 Specific discharge capacity plots of CoMnO/CC assembled ZABs at a current density of 10 mA cm^{-2}.

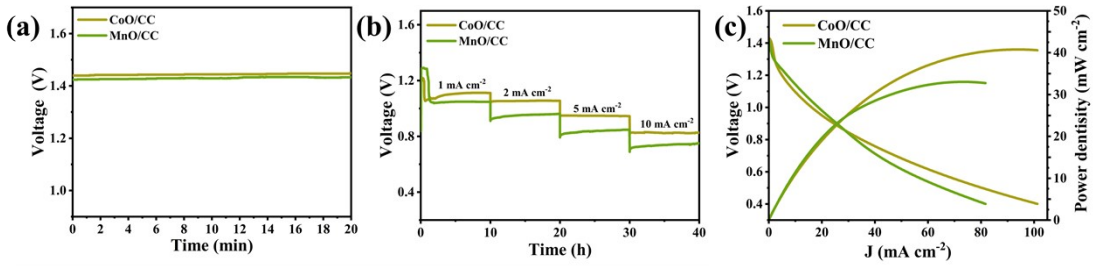

Fig. S12 Zinc-air batteries assembled with CoO/CC and MnO/CC electrodes: (a) open-circuit voltage; (b) discharge voltage step (at current densities of 1~10 mA cm^{-2}); (c) discharge polarization curves and power density curves.

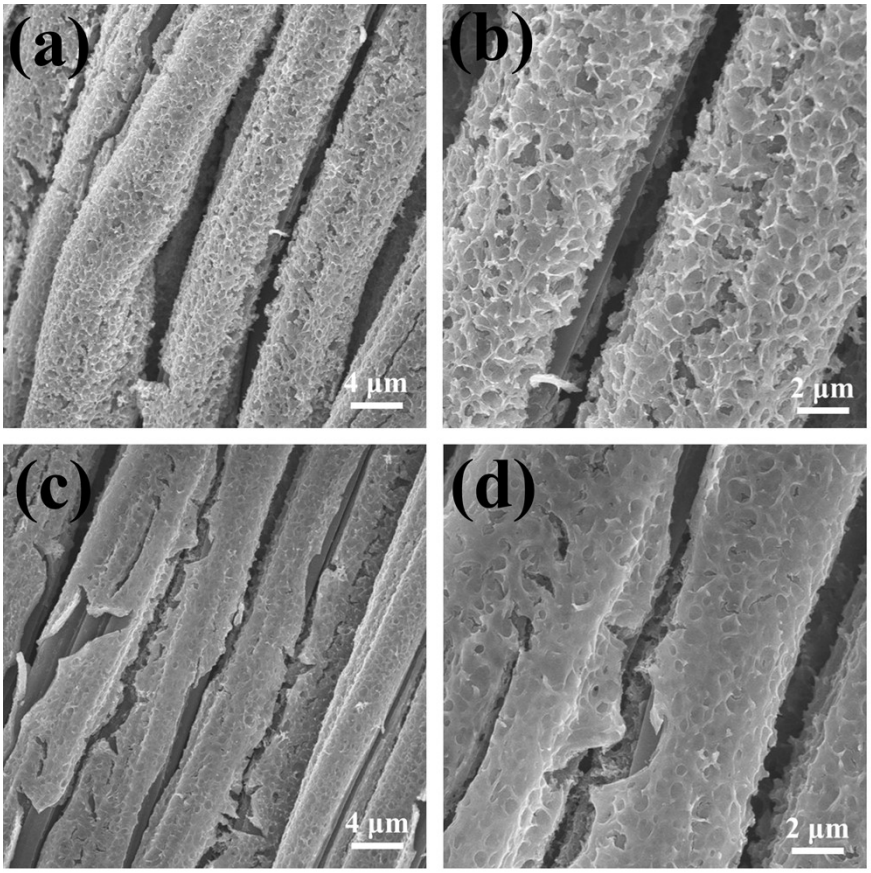

Fig. S13 (a, b) SEM image of CoMnO/CC; (c, d) SEM image of CoMnO/CC after 300 h stability test.

Reference

(S1) Cheng, Y.F.; Liao, F.; Shen, W.; Liu, L.B.; Jiang, B.B.; Li, Y.Q.; Shao, M.W. Carbon cloth supported cobalt phosphide as multifunctional catalysts for efficient overall water splitting and zinc–air batteries. Nanoscale 2017, 9, 18977–18982.

(S2) Liu, Q.; Wang, L.; Liu, X.; Yu, P.; Tian, C.; Fu, H. N-doped carbon-coated Co_3O_4 nanosheet array/carbon cloth for stable rechargeable Zn-air batteries. Sci. China Mater. 2019, 62, 624–632.

(S3) Li, S.X.; Zhang, H.; Wu, L.; Zhao, H.W.; Li, L.X.; Sun, C.G.; An, B.G. Vacancy-engineered CeO_2/Co heterostructure anchored on the nitrogen-doped porous carbon nanosheet arrays vertically grown on carbon cloth as an integrated cathode for the oxygen reduction reaction of rechargeable Zn–air battery. J. Mater. Chem. A 2022, 10, 9858–9868.

(S4) Chen, L.L.; Song, Z.H.; Li, Z.; Yang, Z.; Zhang, J.M.; Li, H.; Zheng, Z.M. Integrated CoO nanoparticles @ porous carbon nanosheets arrays on carbon cloth as cathode for rechargeable Zn-air batteries. J. Alloys Compd. 2022, 894, 162456.

(S5) Yu, N.F.; Shu, X.Y.; Yang, Y.J.; Wang, H.H.; Huang, Q.H.; Tian, N.; Ye, J.L.; Wu, Y.P. In situ growth of N-doped bamboo-like carbon nanotubes embedded with FeNi nanoparticles on carbon cloth as self-standing cathodes for efficient rechargeable zinc–air batteries. Catal. Sci. Technol. 2025, 15, 1604–1616.

(S6) Chen, L.; Yao, R.; Zhang, Y.; Li, W.; Li, J.; Liu, G. Dual doping of W and Cr on Co_3O_4 accelerates reconstruction for improved oxygen evolution in neutral media. J. Alloys Compd. 2025, 184168.

(S7) Guan, Z.; Bo, L.; Zhu, J.; Feng, Z.; Wang, Q.; Li, Y.; Gou, J.M.; Yang, X.L.; Nian, F.; Tong, J. Defect engineering and electronic modulation of heterostructured CoP/Co_3O_4/N-doped carbon nanofibers as efficient bifunctional electrocatalysts for water splitting. J. Colloid Interface Sci. 2025, 138979.

(S8) Lin, Y.; Xu, W.; Gao, Z.; Liang, Y.; Jiang, H.; Li, Z.; Wu, S.L.; Cui, Z.D.; Sun, H.J.; Zhang, H.F.; Zhu, S. Self-supporting high-entropy Co-Cr-Fe-Ni-Nb oxide

electrocatalyst with nanoporous structure for oxygen evolution reaction. Chem. Eng. J. 2024, 489, 151233.

(S9) Zhang, X.; Liu, Y.; Dai, H.; Xu, D.; Chen, Y.; Pan, D.; He, T.; Zhang, Y.; Chen, S.W.; Ouyang, X. Efficient trifunctional electrocatalysts with iron single atoms electronically coupled with adjacent ruthenium nanoclusters for zinc-air battery-powered water splitting. Appl. Catal. B Environ. 2025, 368, 125127.

(S10) Chu, X.; Wang, Y.; Sun, J.; Wu, Y.; Jiang, W.; Liu, B.; Liu, C.B.; Che, G.B.; Sun, Y.T.; Yang, X. Nitrogen-doped carbon nanotube encapsulated CoCu bimetallic alloy particles to promote efficient oxygen evolution reaction via electronic structure regulation. J. Colloid Interface Sci. 2025, 137775.